

# Minimax Current Density Gradient Coils: Analysis of Coil Performance and Heating

Michael S. Poole\*<sup>1</sup>, Peter T. While<sup>2</sup>, Hector Sanchez Lopez<sup>1</sup>, Stuart Crozier<sup>1</sup>

Word Count: 5085

Abbreviated title: Minimax $|j|$  Coil Performance Analysis

<sup>1</sup> School of Information Technology and Electrical Engineering, University of Queensland, St Lucia, Brisbane, Queensland 4072, Australia.

<sup>2</sup> School of Mathematics and Physics, University of Tasmania, Private Bag 37, Hobart, Tasmania 7001, Australia.

\*Corresponding author: Dr. Michael Poole, School of Information Technology and Electrical Engineering, University of Queensland, St. Lucia, Brisbane, QLD 4072, Australia. Tel: +61 7 336 58304, Fax: +61 7 3365 4999, E-mail: michael@itee.uq.edu.au

## Abstract

Standard gradient coils are designed by minimising the inductance or resistance for an acceptable level of gradient field nonlinearity. Recently, a new method was proposed to minimise the maximum value of the current density in a coil additionally. The stated aim of that method was to increase the minimum wire spacing and to reduce the peak temperature in a coil for fixed efficiency. These claims are tested in the present study with experimental measurements of magnetic field and temperature as well as simulations of the performance of many coils. Experimental results show a 90% increase in minimum wire spacing and 40% reduction in peak temperature for equal coil efficiency and field linearity. Simulations of many more coils indicate increases in minimum wire spacing of between 50% and 340% for the coils studied here. This method is shown to be able to increase coil efficiency when constrained by minimum wire spacing rather than switching times or total power dissipation. This increase in efficiency could be used to increase gradient strength, duty cycle or buildability.

## Keywords

Gradient coils,  $\min \max |j|$  current density, temperature, wire spacing, efficiency.

## Introduction

Magnetic resonance images are created by imposing linear gradient fields and encoding spatial information of an object in the frequency and phase of the acquired NMR signal. The gradient fields are generated by gradient coils; coils of wire carrying low frequency currents to play-out myriad pulse sequences. It is generally desirable for the gradient fields to be accurately linear, intense and rapidly switched [1]. Minimum inductance coils [2] ensure fastest possible switching, which is governed by inductance, for a given field linearity and gradient field strength. This approach has been especially successful in the design of whole-body gradient coils and provided improved gradient coils enabling modern rapid imaging sequences. For smaller gradient coils, such as those used in microscopy, the heating due to the resistive power dissipation may limit the gradient strength and a minimum resistance coil design approach is appropriate [3]. Minimum inductance and resistance coils are quite similar and neither approach addresses directly the minimum wire spacing of the coil; an important practical concern that may also limit the gradient strength.

A trivial way to increase the minimum wire spacing is to reduce the number of wires in the coil, but this results in a proportional reduction of the gradient strength. It is simple to include wire spacing constraints in coil design methods that consider discrete wires [4]. However, these methods lack generality with respect to the geometry of coils and their optimisation problem is generally highly non-linear and must be solved by time-consuming stochastic optimisation methods [5] to avoid local minima. Multiple layer coils allow wire spreading in each layer but increases the radial size [6]. Wires paths from the primary coil may be allowed to join with those of the shield coil, either at the ends [7] or in the middle [8] of the coil to help in spreading the closest wires, at the expense of build complexity. With continuous current density coil design methods it is possible to manually specify the current density in regions of a coil with densely packed wires [9, 10, 11]. This requires considerable user input and results in sub-optimal coils. Poole *et al.* developed a method that spreads the closest wires automatically, but again the optimality of the resulting coils was not guaranteed [12]. Recently, Poole *et al.* presented a method to optimally minimise the maximum current density ( $\text{minimax}|j|$ ) of a coil and thereby maximise the minimum spacing between wires [13]. While *et al.* presented a similar approach to reduce the maximum temperature [14] by modelling the temperature distribution [15]. In [13] the maximum current density was added to an otherwise standard optimisation functional (containing field linearity, inductance, resistance, eddy current control and torque-balancing, e.g. Eq. (5) in Ref. [16]) and solved using convex optimisation techniques. This  $\text{minimax}|j|$  method allows all of these terms to be optimised simultaneously yielding a huge range of possible coils with different performance characteristics. It is expected that the most desirable coil for a specific application is some trade-off between minimum inductance and  $\text{minimax}|j|$  (or minimum resistance and  $\text{minimax}|j|$ ). Therefore, it is essential to

the design of gradient coils that this trade-off be studied thoroughly.

In the present study the performances of a suite of  $\text{minimax}|j|$  gradient coils designed with [13] were investigated and two of these coils were compared with empirical results. These experiments were conducted to establish the improvements that are to be expected in the stated aim of the method, namely **reduced maximum current density for fixed field linearity and coil efficiency**. The efficiency of a gradient coil is defined in the present study as the magnitude of the gradient of the magnetic field that is produced by the coil carrying one ampere. Since maximum current density,  $\text{max}|j|$ , is inversely proportional to the minimum wire spacing of a coil design and peak temperature is hypothesised to be commensurate with maximum current density, secondary and tertiary aims may be **reduced peak temperature for fixed field linearity and efficiency** or **increased minimum wire spacing for fixed field linearity and efficiency**.

It is the purpose of the present study to analyse these trade-offs and provide some guidance on the appropriate use and expected gains of the  $\text{minimax}|j|$  approach. X gradient coils with length-to-diameter ratios that vary over a typical range for MRI were studied. Performance figures are compared in order to observe the way in which they change as the  $\text{minimax}|j|$  weighting is varied. This allows us to see what improvement can be gained in efficiency for a given inductance increase, for example. Prototype coils were built and tested in thermal imaging, field mapping and impedance measuring experiments to assess the hypothesis that the peak coil temperature is reduced, the resistance increases and the magnetic field remains the same in practice. Results of thermal simulations show how much the peak temperature can be reduced for a given increase in power dissipation over a range of coils. Ultimately, gradient coils with higher gradient field strengths are expected as a result of using the  $\text{minimax}|j|$  coil design approach which will see a consequential improvement in MRI.

## Methods

First the relevant aspects of the  $\text{minimax}|j|$  technique are reviewed and some repeatedly used terms are established. Then, the experimental methods that we employed in order to study this technique are described.

### Minimising the Maximum Current Density

A gradient coil design method can be considered to be composed of three parts; the method by which the electromagnetic problem is discretised for numerical computation, construction and solution of the optimisation problem yielding the “optimal coil” and finally the conversion of the numerical solution to buildable wire paths.

## Discretising the electromagnetic problem

Gradient coil design is essentially an inversion of the Biot-Savart equation since we consider only magnetostatics. The Biot-Savart equation is linear, therefore a convenient discretisation would produce a linear system of equations relating the magnetic field to the causal current density. If only one component (by definition, the  $z$  component) of the magnetic field,  $B_z(\mathbf{r})$ , is considered and a surface current density,  $\mathbf{J}(\mathbf{r})$ , is assumed, a stream-function (or integrated current) approach [17, 18, 19] can be used.  $B_z(\mathbf{r})$  can subsequently be discretised using the values at particular points or decomposed into spherical harmonics and  $\mathbf{J}(\mathbf{r})$  can be represented as a weighted sum of basis functions:  $\mathbf{J}(\mathbf{r}) = \sum_m^M \psi_m \mathbf{J}_m(\mathbf{r})$ , where  $\mathbf{J}_m(\mathbf{r})$  are the basis functions and  $\psi_m$  are the weights that define the coil. Three types of basis functions were used with the minimax $|j|$  approach in [13] where the current density was either represented as a weighted sum of; truncated sinusoids on a finite-length cylinder [20, 21], locally-linear functions on triangular boundary elements [22] or sinusoidal/linear functions on axi-symmetric boundary elements [10, 23]. The sum of sinusoids (SoS) method was used in the present paper since only simple cylindrical coils were considered.

## Optimisation

Inversion of the Biot-Savart equation is well-known to be an ill-posed inverse problem [24]. Given a specified magnetic field, there are an infinite number of ways in which it can be generated, most of which are not practicable. Optimisation techniques, for example Tikhonov regularisation, must be used in order to choose a practicable coil design. The optimisation functional used in the minimax $|j|$  method [13] is given in Eq. (1)

$$\min_{\psi \in \Psi} \{U(\psi) = f(\psi) + \alpha e(\psi) + \beta W(\psi) + \gamma P(\psi) + \delta \|j(\psi)\|_\infty\} \quad (1)$$

where  $\psi$  is the solution vector,  $\Psi$  is the set with zero net torque,  $f(\psi)$  is the magnetic field error term,  $e(\psi)$  reflects the eddy current control,  $W(\psi)$  is the stored energy,  $P(\psi)$  is the power dissipation,  $\|j(\psi)\|_\infty$  is the maximum current density magnitude and  $\alpha$ ,  $\beta$ ,  $\gamma$  and  $\delta$  are user-definable parameters with which to control the optimisation trade-off. Eq. (1) is solved using convex optimisation techniques with smoothing [25], since  $\partial \|j(\psi)\|_\infty / \partial \psi$  is not defined.

## From $\psi$ to the coil design

The optimisation produces the optimal solution in the form of the vector  $\psi$  which contains the weights and are used with the basis functions,  $\mathbf{J}_m(\mathbf{r})$ , to reconstruct  $\mathbf{J}(\mathbf{r})$  and all dependent properties, for example magnetic field,  $B_z(\mathbf{r})$ , or power dissipation,  $P$ . The wire-paths are determined by  $N_c$  equally-spaced level sets of the stream-function of the current density,  $\psi(\mathbf{r})$  [17, 18, 19].

## Simulation of the Coil Performance

At this point a suite of coils can be designed with varying  $\alpha$ ,  $\beta$ ,  $\gamma$  and  $\delta$  and their predicted performance simulated. The magnetic field from each coil was calculated by applying the elemental Biot-Savart law along the wire paths. The efficiency,  $\eta$  ( $\text{Tm}^{-1}\text{A}^{-1}$ ), was then calculated by least squares fitting to a perfect linear field over the whole region of interest (ROI). The inductance,  $L$ , resistance,  $R$  and magnetic field,  $B_z(\mathbf{r})$ , can also be calculated. Furthermore, accurate  $L$  and  $R$  simulation can be performed using Fasthenry [26] with realistic wire thicknesses.

It is common to quote a figure-of-merit (FoM) for the performance of gradient coils which reflects the requirements of the coil. For whole-body gradient coils, the strength of the gradient field is limited by the desire for rapid switching. In coil design terms, this means that the efficiency is limited by the inductance. In this case, the most common FoM,  $\frac{\eta}{\sqrt{L}}$ , can be used (sometimes used as  $\frac{\eta^2}{L}$  or similar). A larger value of  $\frac{\eta}{\sqrt{L}}$  implies lower power requirement of the gradient amplifiers during switching. However, if it is supposed that our amplifier is powerful enough to drive our coil with the desired switching rate, there may be some difficulty in maintaining large currents in the gradient coils due to excessive heating. In this case  $\eta$  is limited by the resistance of the coil. The appropriate FoM in this case is  $\frac{\eta}{\sqrt{R}}$ . A larger value of  $\frac{\eta}{\sqrt{R}}$  implies that less heat energy is dissipated by the gradient coil per second for a given gradient field strength. Furthermore, the cooling system of a gradient coil may be such that the resulting heat is easily removed, in which case, the efficiency may be limited by the minimum practicable wire spacing of the coil and the appropriate FoM is  $\eta w$ , where  $w$  is the minimum wire spacing of the coil ( $\frac{\eta}{\max|j|}$  may be used equivalently). An essential property of these FoMs is that they are invariant when the number of turns used to make the coil,  $N_c$ , is changed.  $\eta \propto N_c$ ,  $L \propto N_c^2$ ,  $\max|j| \propto N_c$ ,  $w \propto N_c^{-1}$  and  $R \propto N_c^2$  (for fixed layer thickness, see Ref. [12] and Refs. therein for further discussion).

Simulated experiments were devised to characterise the behaviour of the optimal coils when  $\min\max|j|$  is included in the optimisation. In the interests of brevity the experiments are restricted to the study of unshielded, symmetric, cylindrical X gradient coils using a SoS discretisation. Appendix A in Ref. [13] gives details of this method. In all cases in the present study values of  $N = 20$  (number of basis functions in  $z$ ) and  $M = 10$  (number of basis functions in  $\phi$ ) were used, giving a total of 200 sinusoidal basis functions. Peak current occurs in the primary coil of actively shielded gradients, so results are expected to be similar to those of unshielded coils. Z gradient, shim, asymmetric and more exotic coils will behave differently, but X gradients are the most common and interesting case to study.

The magnetic field linearity must be high enough for accurate imaging and is therefore often a fixed specification. Throughout this study the magnetic field error was maintained at  $5.00 \pm 0.01$  % (of the

maximum field in the ROI). The ROI was a cylindrical region with 0.4 m diameter and 0.4 m length and the diameter of the coil was 0.76 m throughout. Firstly,  $W$  was traded for  $\max|j|$  by careful selection of the  $\beta$  and  $\delta$  parameters for  $\alpha = 0$  and  $\gamma = 0$  and 4 different coil lengths were used:  $l = 1.2, 1.4, 1.6$  and  $1.8$  m (resulting in a typical range of coil length-to-diameter ratios). The second experiment differs from the first in that the trade-off is made between  $\max|j|$  and  $P$  rather than  $W$ .

## Prototype Coils for Performance and Heating Tests

In order to validate and calibrate the simulations, prototype coils were produced. These coils correspond to the  $\min(P)$  and  $\min\max|j|$  X gradient coils for  $l = 1.2$  m. Prototype coils of 1:5.28 scale were made for inductance, resistance, magnetic field and temperature experiments. A variable track width was used with a maximum track width of 20 mm and a 1 mm gap was maintained between each wire. A two-layer design was produced to avoid the use of a direct return path that would affect the temperature measurements. Flexible printed circuit boards (PCBs) were manufactured with 0.15 mm thick FR4 (flame retardant class 4, epoxy resin impregnated glass fibre sheet; a standard PCB substrate) and 35  $\mu\text{m}$  copper top and bottom. Coils were potted in epoxy resin (Araldite LY 3600 - Huntsman Advanced Materials, The Woodlands, TX, US) and glass fibre composite with 2.5 mm thickness either side of the PCB. Figure 1 shows the  $\min(P)$  coil before painting with matte white paint. A matte white surface provided a uniform emissivity and avoided thermal reflections as much as possible.

Each coil was connected to 3.0 A DC current supply (GW Instek GPC-3030 - New Taipei City, Taiwan; corrected for temperature dependent resistivity), subject only to unforced radiative and convective cooling and imaged regularly over 40 mins with a thermal imaging camera (NEC F30 - NEC Avio Infrared Technologies, Tokyo, Japan) assuming an emissivity of 1.0. Impedance measurements were made using an impedance meter (HP 4275A - Agilent Technologies, Santa Clara, CA, US) and resistance at thermal equilibrium recorded from the power supply.

Magnetic field maps were obtained by dual echo  $B_0$  mapping sequence data from a 3T MRI scanner (Siemens Tim Trio - Siemens, Erlangen, Germany; 12 channel head coil;  $T_E = 4.92, 7.38$  ms) with a water phantom with and without  $84 \pm 1$  mA DC current in the coil, which was provided by a battery and series ballast resistors. Images were subtracted to obtain the  $B_0$  due to each coil and a linear magnetic field was fitted with rotation, offset and scaling to obtain efficiency and field error measurements of the prototype coils.

## Thermal Simulations

In order to extrapolate the temperature experiments obtained from the two prototype coils, thermal simulations [15] were performed on all other coils for the trade-off between  $\min(P)$  and  $\min\max|j|$ . The thermal characteristics are presented in appendix A and those marked with an asterisk were tuned to fit the experimental data. Fitting was performed because the true parameters were not known and simulated annealing was used with typical material properties as initial guesses. The difference between the simulated and experimental data raised to the power of eight was minimised to ensure a good fit to the  $\max(T)$ . No conclusions are to be drawn from the goodness of fit between simulated and experimental temperature, but fitting the simulation to the experiment gives a realistic basis for comparing the different simulated coils to one another. The thermal properties remained the same for all simulations. This then permits the investigation of the relationship between  $\max|j|$  and  $\max(T)$  for these specific coils and the trade-off between total power dissipation and  $\max(T)$  by scaling the simulated data to the experimentally measured power dissipation.

## Results

### Simulation of the Coil Performance

Fig. 2 shows the results produced by simulating the performance of the 123 different coil designs. Figure 2 A shows the trade-off parameters,  $\beta$ ,  $\gamma$  and  $\delta$ , required to maintain the 5% maximum field error.  $\beta$  is plotted normalised by  $\beta_W$ : the  $\beta$  required to give 5% field error when  $\gamma = \delta = 0$  (i.e a purely stored energy minimised coil). Similarly,  $\gamma$  is normalised by  $\gamma_P$  and  $\delta$  by  $\delta_J$ .

The FoM results for all 123 coils are plotted in Fig. 2 to illustrate the trade-off in performance between optimising for  $\min(W)$  and  $\min\max|j|$ , B, and between  $\min(P)$  and  $\min\max|j|$ , C. These data are presented together in Fig. 2 D inverted and normalised by the FoMs for the standard  $\min(W)$  and  $\min(P)$  coils. This figure allows the prediction of the increase in inductance or resistance that could be expected due to a given increase in wire spacing, for fixed efficiency.

In order to get a clearer picture of the coils behind these performance data, 12 wire patterns are shown in Fig. 3. For each different length,  $l = 1.2, 1.4, 1.6$  and  $1.8$ , a standard minimum power coil is displayed (left column) alongside two other coils with  $\delta/\delta_J$  approaching 1 (right column) and one somewhere towards the middle of the trade-off between  $\min(P)$  and  $\min\max|j|$  (central column). The region in which  $|j|$  is within 5% of  $\max|j|$  is shaded orange. Furthermore, these coils are labelled on the FoM graphs in Figure 2.

## Prototype Coils for Performance and Heating Tests

Processed magnetic field maps of the small-scale prototype coils are shown in Fig 4 for the  $\min(P)$ , A, and  $\min\max|j|$ , B, coils. The magnetic field maps are shown in the  $x$ - $z$  plane for  $y = 0$  as contour plots (solid green lines), with a fitted linear field superimposed (dashed blue lines). 5% field error between the experimentally-obtained field and its linear fit are added (thick red lines) along with the outline of the region of uniformity, ROU, (orange box) and the extents of the coil (thick black line).

The coil efficiencies of the full-scale coils obtained by scaling the efficiencies of both prototype coils from linear fitting the magnetic field maps were measured to be  $(1.48 \pm 0.07) \times 10^{-5} \text{ Tm}^{-1}\text{A}^{-1}$ . The error was calculated from an estimated maximum radial manufacturing error of 0.5 mm and a maximum drift of 0.5 mA in the current provide by the gel cell. From Biot-Savart integration of the wire paths, the coil efficiencies were calculated to be 1.51 and  $1.50 \times 10^{-5} \text{ Tm}^{-1}\text{A}^{-1}$  for the  $\min(P)$  and  $\min\max|j|$  coils respectively.

Temperature data obtained from thermal imaging and simulation are displayed in Fig. 5 for both of the prototype coils built. The temperature simulations were warped to a cylindrical shape to match the thermal imaging data qualitatively. These results are quantitatively compared, shown in Fig. 6, where the measured and simulated temperatures of the  $\min(P)$  and  $\min\max|j|$  coils are plotted for axial position,  $\phi = 0, 45^\circ$  and  $90^\circ$ . The maximum temperature,  $\max(T)$ , increase during the heating phases approaching thermal equilibrium is shown in Fig. 7 for both coils and the ambient temperature,  $T_{\text{amb}}$ . Exponential fits of the form  $T(t) = T_{\text{amb}} + (\max(T) - T_{\text{amb}})(1 - e^{-t/\tau})$  were made to the data to estimate  $\max(T)$ .  $\tau$  is a decay constant fitted to the data.

## Thermal Simulations

The thermal and performance simulations were collected and compared with the experimental data in Fig. 8. To give the power dissipated,  $P$ , each coil was simulated with Fasthenry at the prototype scale and the resistance was multiplied by the square of the current needed in each coil so as to produce the same magnetic field as the  $\min(P)$  prototype coil carrying 3 Amp ( $G = 45 \text{ mTm}^{-1}$ ). The simulated  $\max(T)$  in each coil is plotted against  $P$  in Fig. 8 A. In order to see whether minimisation of the peak current density is a sensible analogue for the reduction of  $\max(T)$  in the coil, the  $\max(T)$  is plotted as a function of the  $\max|j|$  in Fig. 8 B.

# Discussion

## Coil Performance

As expected, the maximum current density in every coil designed with  $\text{minimax}|j|$  is reduced with respect to the standard  $\text{min}(W)$  and  $\text{min}(P)$  coils. One aim of the present study was to find what reduction in  $\text{max}|j|$  could be achieved over a range of different lengths and what the consequential change in other parameters of the coil are. Gradient coil design is a multi-objective optimisation problem and as such we should characterise all the possible coils to understand fully the nature of the trade-off between the objectives. The magnetic field linearity objective was removed as a variable by fixing the maximum field error to 5% in all cases. Mathematically, a more rigorous constraint would be to fix the  $\ell^2$ -norm of the field error to a certain value since this is the objective in the optimisation (1). This is not a convenient measure for coil designers however. In the case of the shorter coils designed here ( $l/d \lesssim 2$ ), the parameters  $\beta$ ,  $\gamma$  and  $\delta$  required to maintain 5% field linearity are close to being a linear trade-off, see Fig. 2 A. This indicates that the objectives of  $\text{min}(W)$ ,  $\text{min}(P)$  and  $\text{minimax}|j|$  compete directly against the field linearity objective in a similar way. However, for longer coils, an unexpected relationship between the parameters was observed; adding  $\text{minimax}|j|$  weighting to the objective functional actually required increases in the  $\text{min}(W)$  and  $\text{min}(P)$  weighting parameters,  $\beta$  and  $\gamma$ , in order to maintain 5% maximum field error. The exact origins of this effect are unknown, but it is our opinion that adding a small amount of  $\text{minimax}|j|$  to the standard  $\text{min}(W)$  and  $\text{min}(P)$  coils actually improves the field linearity in longer coils. For coils close to the  $\text{min}(W)$  and  $\text{min}(P)$  solutions, the amounts of sinusoids with high spacial frequency have tended to zero and so the performance of these coils is not limited by the finite number of sinusoids used. For the coils with more  $\text{minimax}|j|$  weighting this is not the case and the performance of these coils is slightly limited by finite  $N$  and  $M$ .

Figures-of-merit (FoMs) were used to analyse the coil performance with respect to stored energy ( $\frac{\eta}{\sqrt{L}}$ ), power dissipation ( $\frac{\eta}{\sqrt{R}}$ ) and maximum current density ( $\eta w$ ) and are plotted for all 123 coils in Figs. 2 B and C. The curvature of these plots provide information of the multi-objective optimality of the intermediate solutions. For example, if a straight line resulted, it would indicate that the two objectives were mutually exclusive. What was found in the present study was that there is a high degree of curvature, which indicates that intermediate solutions provide results with a high degree of optimality in both metrics. Such behaviour is well known in the subject of regularisation of ill-posed problems in the study of the L-curve.

Figure 2 D provides a means by which to estimate the increase in inductance or resistance one might expect for a given increase in wire spacing over the standard  $\text{min}(W)$  and  $\text{min}(P)$  solutions (which appear at [1,1] on this graph). The relative increase in minimum wire spacing achievable appears to decrease as the coil gets longer, as has been observed in previous work [27]. However, for the longest coil a greater degree of wire

spreading is achieved, which is an unexpected result that deserves more thorough investigation. The black line in Fig. 2 D gives an example for a  $\min(P)$  coil with a length of 1.2 m; an increase of approximately 70% in minimum wire spacing would result in an increase in resistance of approximately 10%, for fixed efficiency. The gains are considerably steeper for the  $\min(W)$  coils since those coils tend to have a small region of very high current density that is very rapidly spread by the addition of a small  $\min\max|j|$  weighting.

## Wire Patterns

Wire patterns of 12 of the coils are shown in Fig. 3 which are labelled correspondingly on Figs. 2 A and C and Fig. 8 A. The coils on the left are standard  $\min(P)$  coils exhibiting typical smooth wire patterns with small regions of high current density. These regions occur at the far ends of the coil for short coils and towards the middle for longer coils. As  $\min\max|j|$  is introduced, those regions of high current density begin to spread and new regions appear in which the current density is maximal. Such cases are shown in the central column, which were chosen as optimal in terms of both total power dissipation and peak temperature from the curves in Fig. 8 A. These wire-patterns appear qualitatively similar to coils presented in [14]. The right column represents coils as we approach the extreme  $\min\max|j|$  coils with little  $\min(P)$  weighting. The shape of their wire patterns are characterised by large regions of equally-spaced parallel wires with more sharp corners and smaller loops to ensure that the field error remains at 5%. More extreme  $\min\max|j|$  coils are possible, but they tend to possess isolated loops and reversed turns for little increase in wires spacing and as such are not of practical interest. This effect indicates that the  $\min\max|j|$  term does not provide a regularising effect on the ill-posed coil design problem and so some regularisation with either the  $\min(W)$ ,  $\min(P)$  or indeed unweighted Tikhonov regularisation is still recommended.

## Magnetic Field Mapping

The theoretical properties of the  $\min\max|j|$  coils demonstrate the increased wire spacing for fixed efficiency and a maximum field error of 5%. Two coils, 3 **a** and **c**, were chosen to be built as small-scale prototypes and have their performance tested. The magnetic fields that these two coils generated are shown in Fig. 4. The contours of the magnetic field appear at an angle due to slight errors in the coil alignment with respect to the scanner coordinate system which was accounted for in the fitting procedure. The 5% field error line was calculated from the difference between the linear fit and the measured field. As demonstrated by the presented data, the field in the ROU deviates exactly by 5% maximally and there is no appreciable difference between the magnetic fields of the  $\min(P)$  and  $\min\max|j|$  coils in this region. From Biot-Savart simulation the fields become clearly different closer to the coil surface well outside the ROU. The measured

coil efficiencies matched the theoretical values within the experimental error.

## Coil Temperature

Temperature measurements and simulations were also made of the two prototypes in order to test our hypothesis that reducing the  $\max|j|$  will reduce the  $\max(T)$ . For a fair experimental heating test, the coils were built in exactly the same way without the presence of any other coil and with a double layer coil design. Thin copper ( $35 \mu\text{m}$ ) was used so that an appreciable temperature rise was observed under safe laboratory conditions and relatively low currents. The double layer design eliminates the need for a return path, which can act as a “heat pipe” removing the heat from the coil, which previously caused unfair comparison of peak temperature measurements [27]. Temperature measurements and simulations of the two prototype coils are presented in Figs. 5, 6 and 7 and used in Fig. 8. Clearly, in the studied prototypes there was a significant reduction in the maximum temperature from both measurement and simulation. Qualitatively, the simulations match the experimental measurements, but quantitatively, there are some differences. This is thought to be as a result of uncertainty in the values for the thermal properties of the prototype materials and an inability of the simulations to model accurately the radiative heat transfer and anisotropic thermal conductivity of the coil layer. In reality, heat is conducted around the coil by the copper tracks, which is not considered in the simulation (instead, an effective thermal conductivity was considered for the coil layer) [15]. The temporal increase in temperature tended towards an equilibrium value,  $\max(T)$  which was estimated by fitting a single exponential function to the data. The fit is poor during the rapid heating phase immediately after the current is switched in, but the fit was only used to estimate  $\max(T)$ . A difference in  $\max(T)$  of  $27 \text{ }^\circ\text{C}$  between  $\min(P)$  and  $\min\max|j|$  designs was observed corresponding to a 40% reduction. In a full scale gradient coil with active cooling, other gradient layers and considerably more current, this reduction will differ, but it is unlikely that in any real coil,  $\max(T)$  in a  $\min\max|j|$  gradient coil would ever be higher than a standard  $\min(P)$  coil.

It was expected that the results shown in Fig. 8 A would present a similar smooth L-curve to Fig. 2 C, but the results produced a curve with a very pronounced corner. This indicates that the coils at the corners are optimal in both measures of coil performance. In other words, if the coil at the corner is chosen, it is expected to have a maximal reduction in peak temperature without actually increasing the total power dissipation. In fact, the properties of the intermediate coils, **b**, **e**, **h** and **k** are as good as, and in some cases better than, the extreme  $\min(P)$  and  $\min\max|j|$  coils; a surprising result. It is thought that the difference in theoretical and real power dissipation originates from the conversion from continuous current density to discrete, variable-thickness tracks and the necessity for a finite gap between tracks [12]. For example, if our

manufacturing method is capable of producing a 1 mm gap between tracks, then a  $\min(P)$  coil with  $w = 2.1$  mm will have tracks at least 1.1 mm wide. An equivalent  $\min\max|j|$  coil with  $w = 3.6$  mm will have at least 2.6 mm thick tracks; the theoretical  $w$  is 70% higher, but the actual tracks are 140% wider. Even though this occurs in localised regions of the coil, it is enough to alter the overall coil resistance dramatically. The measured resistance and temperature data of the prototype coils are plotted on Fig. 8. The measured resistance of the two coils were larger than the simulated results, which may be caused by the presence of solder joints, interconnections and slightly different copper thicknesses and resistivities.

The relationship between  $\max(T)$  and  $\max|j|$  shown in Fig. 8 B demonstrates generally that a reduction in  $\max|j|$  causes a reduction of  $\max(T)$ , but that the effect is not entirely linear. Towards the extreme  $\min\max|j|$  coils no decrease in  $\max(T)$  was found, and in some cases a slight increase. This additionally contributes to the pronounced corner of the L-curve in Fig. 8 A and proves that the best coil is one that has some degree of  $\min\max|j|$  but is still relatively smooth from a significant  $\min(P)$  or  $\min(W)$  weighting.

## Conclusions

The  $\min\max|j|$  method can be used to increase the efficiency of gradient coils for a given minimum wire spacing, with a consequential small increase in resistance and stored-energy. This may be useful for small coils in which the coil design is not dominated by the required switching time or total power dissipation. The resistance increase is less in practice than in theory due to the necessity for a finite gap between wire tracks. The trade-off between  $\min\max|j|$  and  $\min(W)$  and  $\min(P)$  is non-linear and as such a “best of both worlds” coil can be found at the part of the curve with maximum curvature and not at either extreme. The location of this coil depends on many factors such as the coil type, length, radius and linearity requirements. The addition of active shielding to the optimisation is necessary for practical gradients and was described in Ref. [13]. It also affects the optimisation trade-off, but was not included in this study.

The maximum temperature in a coil can be significantly reduced with a small amount of  $\min\max|j|$  weighting,  $\delta$ . The  $\max(T)$  was found to be commensurate with  $\max|j|$ , justifying the use of the  $\min\max|j|$  approach for the reduction of  $\max(T)$ . This relationship is not linear and as  $\max|j|$  is reduced the total power is increased which, at some point in the trade-off, counteracts the effect of reduced  $\max|j|$  though thermal conduction of the heat throughout the coil. Again, quantitative reductions in peak temperature are expected to vary widely for different types of gradient coil.

## **Acknowledgements**

The authors wish to acknowledge Don Maillet for his assistance in obtaining the scan data for the field mapping, Iwao Nakajima for the concept of the double layer PCB design without return paths, Ewald Weber for assistance in PCB production and Kimberley Nunes and the reviewers for greatly improving the quality of the final article. This project was funded by MedTeQ; a Queensland government smart state initiative.

## References

- [1] R. Turner. Gradient Coil Design: A Review Of Methods. *Magnetic Resonance Imaging*, **11**(7), 903–920, (1993).
- [2] R. Turner. Minimum Inductance Coils. *Journal of Physics E: Scientific Instruments*, **21**(10), 948–952, (1988).
- [3] R. Bowtell and P. Mansfield. Minimum Power, Flat Gradient Pairs for NMR Microscopy. *Proceedings of the International Society for Magnetic Resonance in Medicine*, **9**, 977, (1989).
- [4] S. Shvartsman and M. C. Steckner. Discrete Design Method of Transverse Gradient Coils for MRI. *Concepts in Magnetic Resonance Part B: Magnetic Resonance Engineering*, **31B**(2), 95–115, (2007).
- [5] S. Crozier and M. Doddrell. Gradient Coil Design by Simulated Annealing. *Journal of Magnetic Resonance Series A*, **103**, 354–357, (1993).
- [6] Bowtell and Robyr. Multilayer Gradient Coil Design. *Journal of Magnetic Resonance*, **131**(2), 286–294, (1998).
- [7] S. Shvartsman, M. Morich, G. Demeester, and Z. Zhai. Ultrashort Shielded Gradient Coil Design with 3D Geometry. *Concepts in Magnetic Resonance Part B: Magnetic Resonance Engineering*, **26B**(1), 1–15, (2005).
- [8] M. Poole, R. Bowtell, D. Green, S. Pittard, A. Lucas, R. Hawkes, and A. Carpenter. Split gradient coils for simultaneous PET-MRI. *Magnetic Resonance in Medicine*, **62**(5), 1106–1111, (2009).
- [9] R. A. Compton. Gradient-Coil Apparatus for a Magnetic Resonance System, *US Patent*, 4,456,881, (1984).
- [10] G. N. Peeren. *Stream Function Approach For Determining Optimal Surface Currents*. PhD thesis, Technische Universiteit Eindhoven, (2003).
- [11] G. Shou, L. Xia, F. Liu, M. Zhu, Y. Li, and S. Crozier. MRI Coil Design Using Boundary-Element Method With Regularization Technique: A Numerical Calculation Study. *Magnetics, IEEE Transactions on*, **46**(4), 1052–1059, (2010).
- [12] M. Poole, H. Sanchez Lopez, and S. Crozier. Adaptively Regularised Gradient Coils for Reduced Local Heating. *Concepts in Magnetic Resonance Part B: Magnetic Resonance Engineering*, **33B**(4), 220–227, (2008).

- [13] M. Poole, P. Weiss, H. S. Lopez, M. Ng, and S. Crozier. Minimax current density coil design. *Journal of Physics D: Applied Physics*, **43**(9), 095001 (13pp), (2010).
- [14] P. T. While, L. K. Forbes, and S. Crozier. Designing gradient coils with reduced hot spot temperatures. *Journal of Magnetic Resonance*, **203**(1), 91–99, (2010).
- [15] P. T. While, L. K. Forbes, and S. Crozier. Calculating temperature distributions for gradient coils. *Concepts in Magnetic Resonance Part B: Magnetic Resonance Engineering*, **37B**(3), 146–159, (2010).
- [16] M. Poole and R. Bowtell. Novel Gradient Coils Designed Using a Boundary Element Method. *Concepts in Magnetic Resonance Part B: Magnetic Resonance Engineering*, **31B**, 162–175, (2007).
- [17] M. J. E. Golay. Magnetic Field Control Apparatus, *US Patent*, 3,515,979, (1970).
- [18] W. Edelstein and F. Schenck. Current Streamline Method for Coil Construction, *US Patent*, 4,840,700, (1989).
- [19] M. A. Brideson, L. K. Forbes, and S. Crozier. Determining Complicated Winding Patterns for Shim Coils Using Stream Functions and the Target-Field Method. *Concepts in Magnetic Resonance*, **14**(1), 9–18, (2002).
- [20] Z. J. J. Stekly. Continuous, Transverse Gradient Coils With High Gradient Uniformity. *Proceedings of the Society for Magnetic Resonance in Medicine*, **4**, 1121, (1985).
- [21] J. W. Carlson, K. A. Derby, K. C. Hawryszko, and M. Weideman. Design And Evaluation Of Shielded Gradient Coils. *Magnetic Resonance in Medicine*, **26**(2), 191–206, (1992).
- [22] S. Pissanetzky. Minimum Energy MRI Gradient Coils of General Geometry. *Measurement Science and Technology*, **3**(7), 667–673, (1992).
- [23] M. Poole and R. Bowtell. Azimuthally Symmetric IBEM Gradient and Shim Coil Design. *Proceedings of the International Society for Magnetic Resonance in Medicine*, **16**, 345, (2008).
- [24] K. Adamiak. Method of the magnetic field synthesis on the axis of cylinder solenoid. *Applied Physics A: Materials Science & Processing*, **16**(4), 417–423, (1978).
- [25] Y. Nesterov. Smooth minimization of non-smooth functions. *Mathematical Programming*, **103**(1), 127–152, (2005).
- [26] M. Kamon, M. J. Tsuk, and J. K. White. FASTHENRY: A Multipole-Accelerated 3-D Inductance Extraction Program. *IEEE Transactions on Microwave Theory and Techniques*, **42**, 1750–1758, (1994).

- [27] M. Poole, P. While, H. Sanchez Lopez, L. Forbes, and S. Crozier. Behaviour of Gradient Coils Designed With Varying Degrees of Minimised Maximum Current Density. *Proceedings of the International Society for Magnetic Resonance in Medicine*, **19**, 3781, (2011).

## List of Figures

|   |  |    |
|---|--|----|
| 1 | Photograph of the $\min(P)$ prototype coil with $N_c = 20$ before painting. . . . .  | 21 |
| 2 | Input and performance data of the trade-off between both $\min(P)$ and $\min(\max j )$ , and $\min(W)$ and $\min(\max j )$ . Trade-off parameters required in order to maintain 5% field error are shown in A normalised by the extreme values. B and C show the $\min(\max j )$ FoM as a function of the $\min(W)$ and $\min(P)$ FoMs respectively. FoMs are inverted and normalised against the $\min(W)$ and $\min(P)$ values and plotted in D to allow estimation of the increase in $W$ or $P$ to be expected for a given increase in minimum wire spacing. . . . . | 22 |
| 3 | Wire-path centres of one quadrant of X gradient coils designed with varying amounts of $\min(P)$ and $\min(\max j )$ , shown with $N_c = 10$ , for total lengths of 1.2 m ( <b>a-b</b> ), 1.4 m ( <b>d-f</b> ), 1.6 m ( <b>g-i</b> ), 1.8 m ( <b>j-l</b> ). The left column shows the $\min(P)$ coils, the right column show $\min(\max j )$ dominated coils and the central column are those coils at the corners of the L-curves in Fig. 8 A. . . . .  | 23 |
| 4 | Magnetic field maps of the $\min(P)$ , A, and $\min(\max j )$ , B, coil prototypes with wire patterns shown in Fig. 3 A and C respectively. Shown are the coil cross-section (thick black line), ROU (orange shaded region), magnetic field $10\mu\text{T}$ contour lines (thin green lines), linear fit contour lines (thin blue dashed lines) and the 5% field error contour (red lines). . . . .  | 24 |
| 5 | Thermal image and simulated data of the $\min(P)$ and $\min(\max j )$ coils at $0^\circ$ and $90^\circ$ rotation. Simulated data was warped to a cylindrical surface to match experimental data. Maximum temperature is given on the colour bar. . . . .   | 25 |
| 6 | Measured and simulated temperature of the $\min(P)$ , $\min(\max j )$ coils along the $z$ direction for azimuthal positions, $\phi$ , $0^\circ$ , A, $45^\circ$ , B and $90^\circ$ , C. . . . .  | 25 |
| 7 | Measured maximum temperature of the $\min(P)$ , $\min(\max j )$ coils and the ambient temperature over time during heating. Single exponential fits are shown as used to estimate the maximum temperature at thermal equilibrium and dotted lines indicate the switching on and off of the current in the coils. . . . .   | 26 |
| 8 | Measured and simulated maximum temperature versus total power dissipation in the coils, A. All coils shown in Fig. 3 are labelled and inset shows data for the two longest coils in detail. Maximum temperature is plotted against maximum current density in B. Linear fits are added to the data in B. . . . .   | 26 |

## List of Symbols

$\psi$  Greek lower case psi,

$\Psi$  Greek upper case psi,

$\alpha$  Greek lower case alpha,

$\beta$  Greek lower case beta,

$\gamma$  Greek lower case gamma,

$\delta$  Greek lower case delta,

$\|\cdot\|_\infty$  double vertical bars, subscript infinity symbol,

$\partial$  Partial differential symbol,

$\eta$  Greek lower case eta,

$\propto$  proportional to symbol,

$\lesssim$  Less than or approximately equal to,

$\ell^2$  curly letter l squared,

$\tau$  Greek lower case tau,

$\phi$  Greek lower case phi,

$\frac{\eta}{\sqrt{L}}$  Greek lower case eta divided by the square root of L,

$\frac{\eta}{\sqrt{R}}$  Greek lower case eta divided by the square root of R,

## Appendix A

| Thermal Property  | Value                                   |
|---|---|
| Copper mass density   | 8960 kg m <sup>-3</sup>                 |
| Copper specific heat capacity                               | 385 J kg <sup>-1</sup> K <sup>-1</sup>  |
| Copper resistivity  | 1.68×10 <sup>-8</sup> Ω m               |
| Copper thermal conductivity                                 | 401 W m <sup>-1</sup> K <sup>-1</sup>   |
| FR4 mass density  | 1900 kg m <sup>-3</sup>                 |
| FR4 specific heat capacity                                  | 1200 J kg <sup>-1</sup> K <sup>-1</sup> |
| FR4 thermal conductivity                                    | 0.23 W m <sup>-1</sup> K <sup>-1</sup>  |
| Coil layer thermal conductivity*                            | 226.8 W m <sup>-1</sup> K <sup>-1</sup> |
| Epoxy mass density  | 1800 kg m <sup>-3</sup>                 |
| Epoxy specific heat capacity                                | 940 J kg <sup>-1</sup> K <sup>-1</sup>  |
| Epoxy thermal conductivity*                                 | 0.234 W m <sup>-1</sup> K <sup>-1</sup> |
| Convective heat transfer coefficient (inner)*               | 5.178 W m <sup>-2</sup> K <sup>-1</sup> |
| Convective heat transfer coefficient (outer)*               | 7.178 W m <sup>-2</sup> K <sup>-1</sup> |
| Radiative heat transfer coefficient (inner)                 | 0 W m <sup>-2</sup> K <sup>-1</sup>     |
| Radiative heat transfer coefficient (outer, min( $P$ ))     | 8 W m <sup>-2</sup> K <sup>-1</sup>     |
| Radiative heat transfer coefficient (outer, minimax $ j $ ) | 7 W m <sup>-2</sup> K <sup>-1</sup>     |
| Surface emissivity  | 0.94                                    |
| Ambient temperature   | 19 °C                                   |

Table 1: Thermal properties assumed for the temperature simulations (\* tuned using simulated annealing).



Figure 1: Photograph of the  $\min(P)$  prototype coil with  $N_c = 20$  before painting.

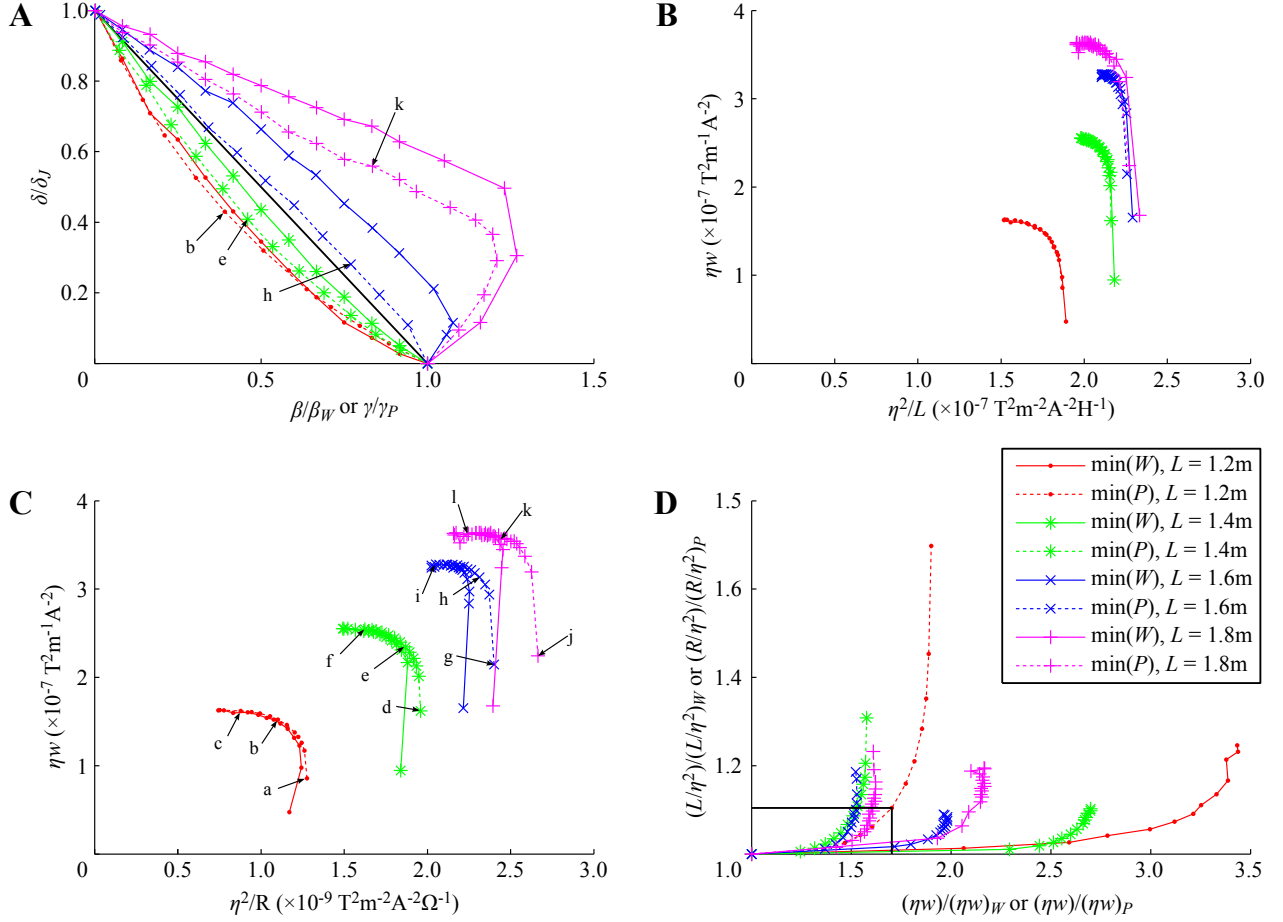


Figure 2: Input and performance data of the trade-off between both  $\min(P)$  and  $\min(\max|j|)$ , and  $\min(W)$  and  $\min(\max|j|)$ . Trade-off parameters required in order to maintain 5% field error are shown in A normalised by the extreme values. B and C show the  $\min(\max|j|)$  FoM as a function of the  $\min(W)$  and  $\min(P)$  FoMs respectively. FoMs are inverted and normalised against the  $\min(W)$  and  $\min(P)$  values and plotted in D to allow estimation of the increase in  $W$  or  $P$  to be expected for a given increase in minimum wire spacing.

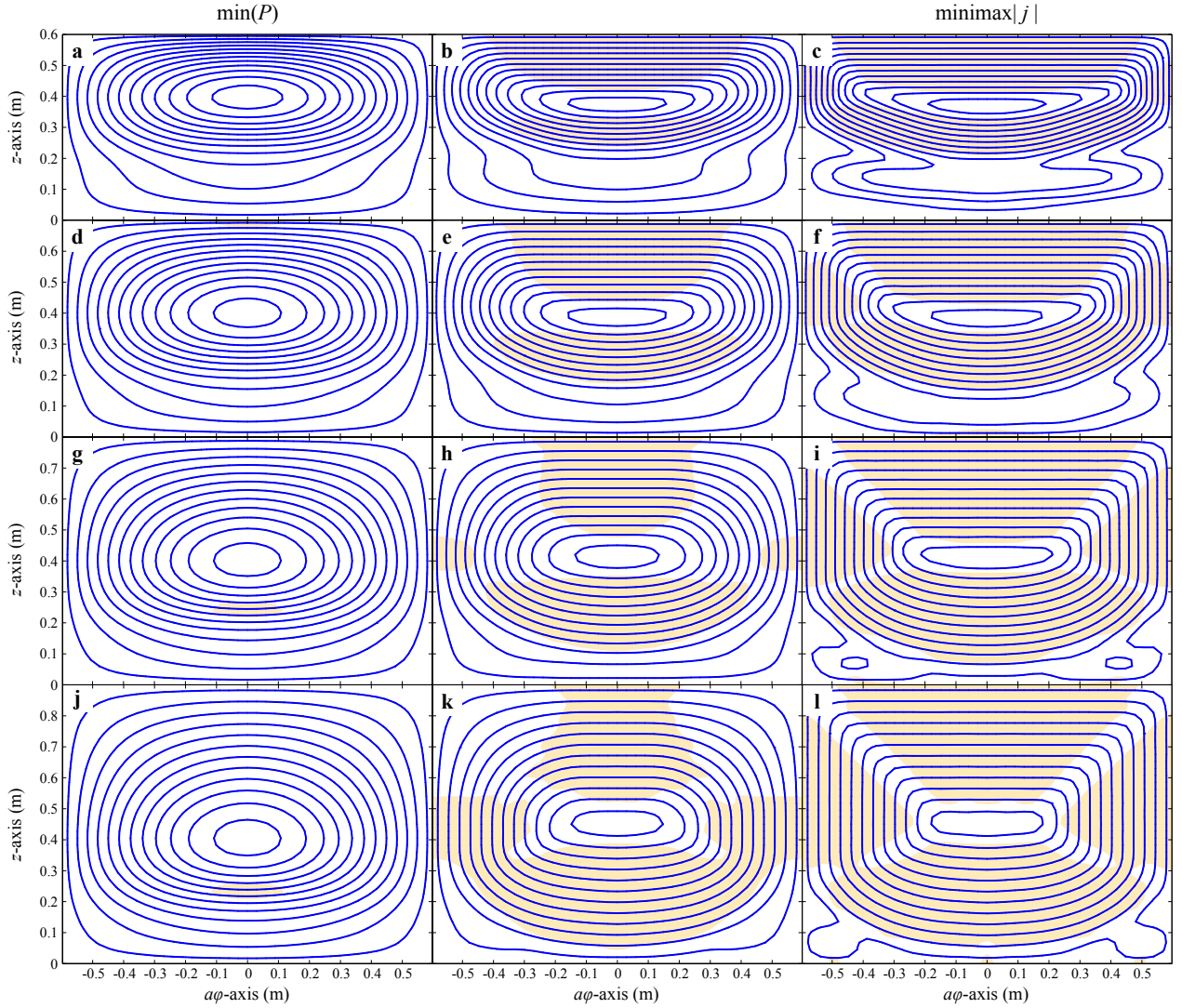


Figure 3: Wire-path centres of one quadrant of X gradient coils designed with varying amounts of  $\min(P)$  and  $\minimax|j|$ , shown with  $N_c = 10$ , for total lengths of 1.2 m (a-b), 1.4 m (d-f), 1.6 m (g-i), 1.8 m (j-l). The left column shows the  $\min(P)$  coils, the right column show  $\minimax|j|$  dominated coils and the central column are those coils at the corners of the L-curves in Fig. 8 A.

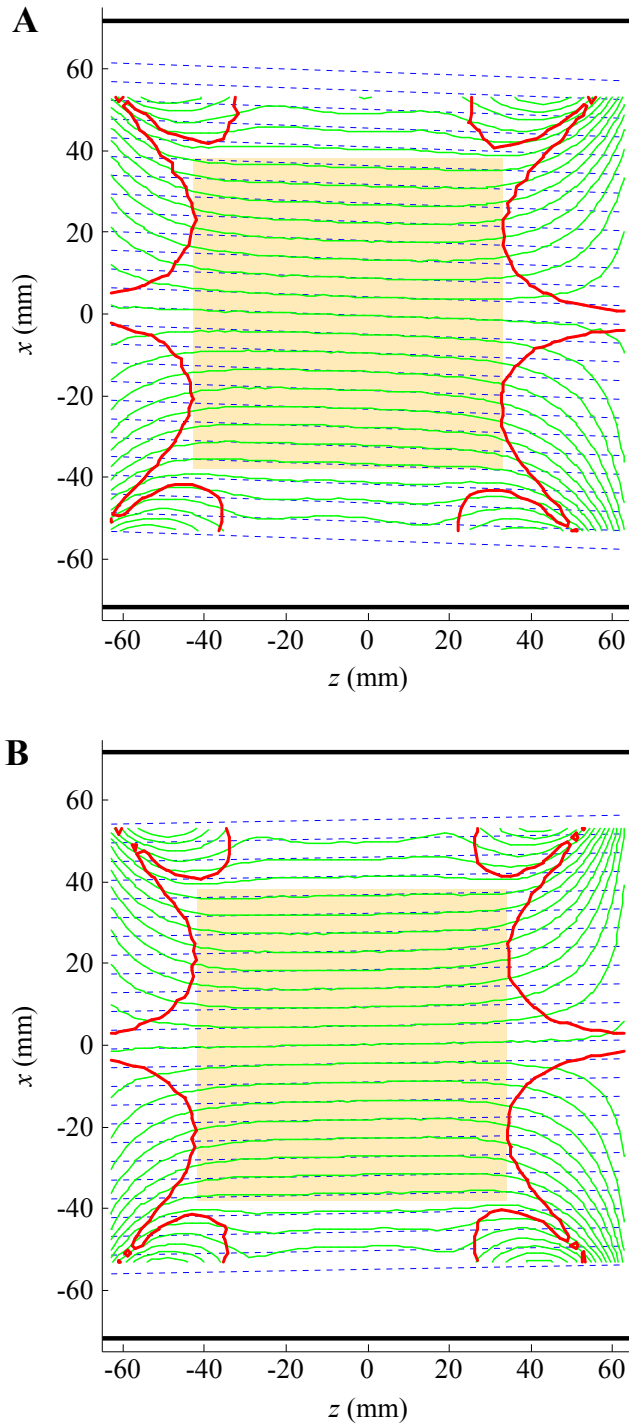


Figure 4: Magnetic field maps of the  $\min(P)$ , A, and  $\min\max|j|$ , B, coil prototypes with wire patterns shown in Fig. 3 A and C respectively. Shown are the coil cross-section (thick black line), ROU (orange shaded region), magnetic field  $10\mu\text{T}$  contour lines (thin green lines), linear fit contour lines (thin blue dashed lines) and the 5% field error contour (red lines).

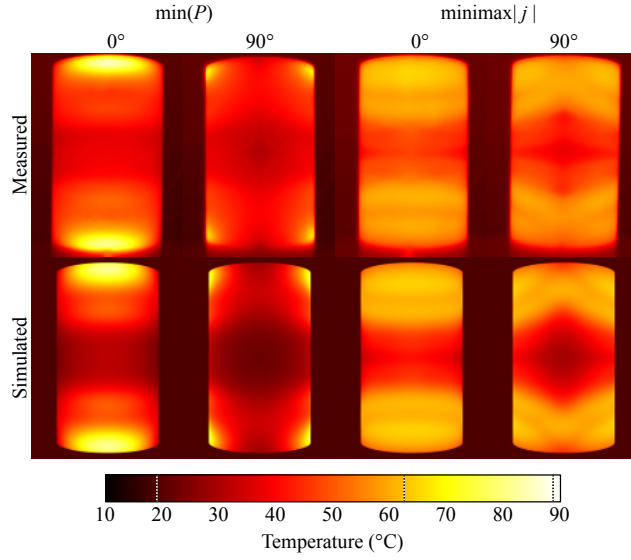


Figure 5: Thermal image and simulated data of the  $\min(P)$  and  $\text{minimax}|j|$  coils at  $0^\circ$  and  $90^\circ$  rotation. Simulated data was warped to a cylindrical surface to match experimental data. Maximum temperature is given on the colour bar.

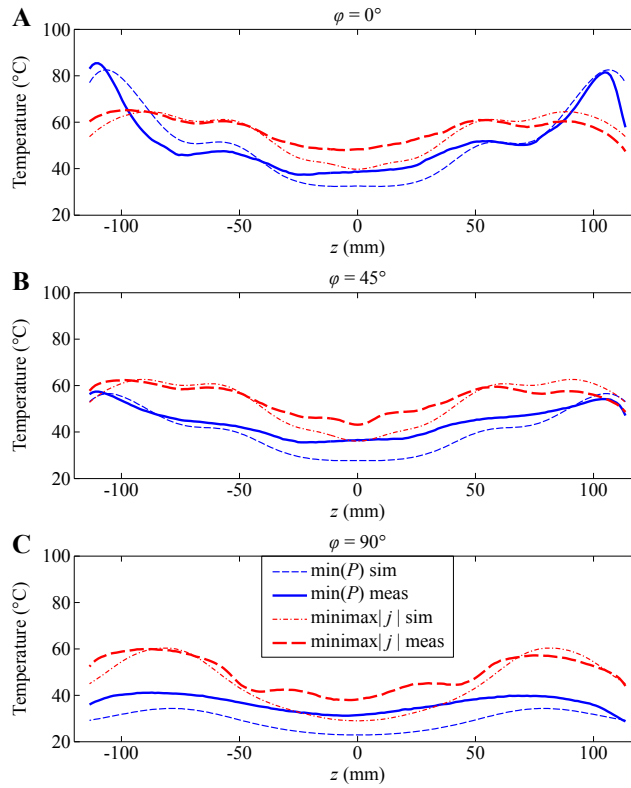


Figure 6: Measured and simulated temperature of the  $\min(P)$ ,  $\text{minimax}|j|$  coils along the  $z$  direction for azimuthal positions,  $\phi$ ,  $0^\circ$ , A,  $45^\circ$ , B and  $90^\circ$ , C.

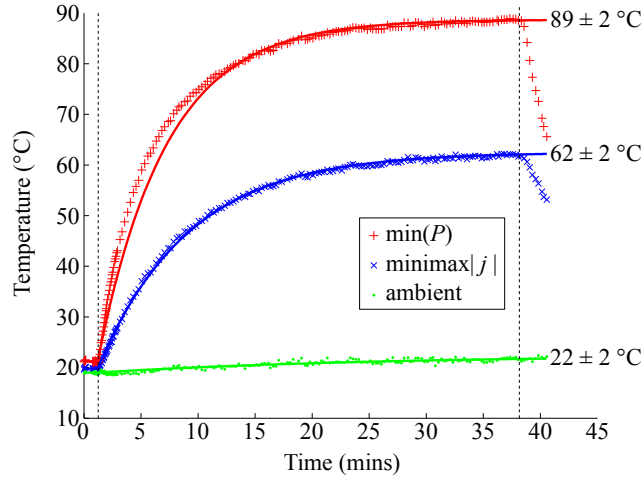


Figure 7: Measured maximum temperature of the  $\min(P)$ ,  $\text{minimax}|j|$  coils and the ambient temperature over time during heating. Single exponential fits are shown as used to estimate the maximum temperature at thermal equilibrium and dotted lines indicate the switching on and off of the current in the coils.

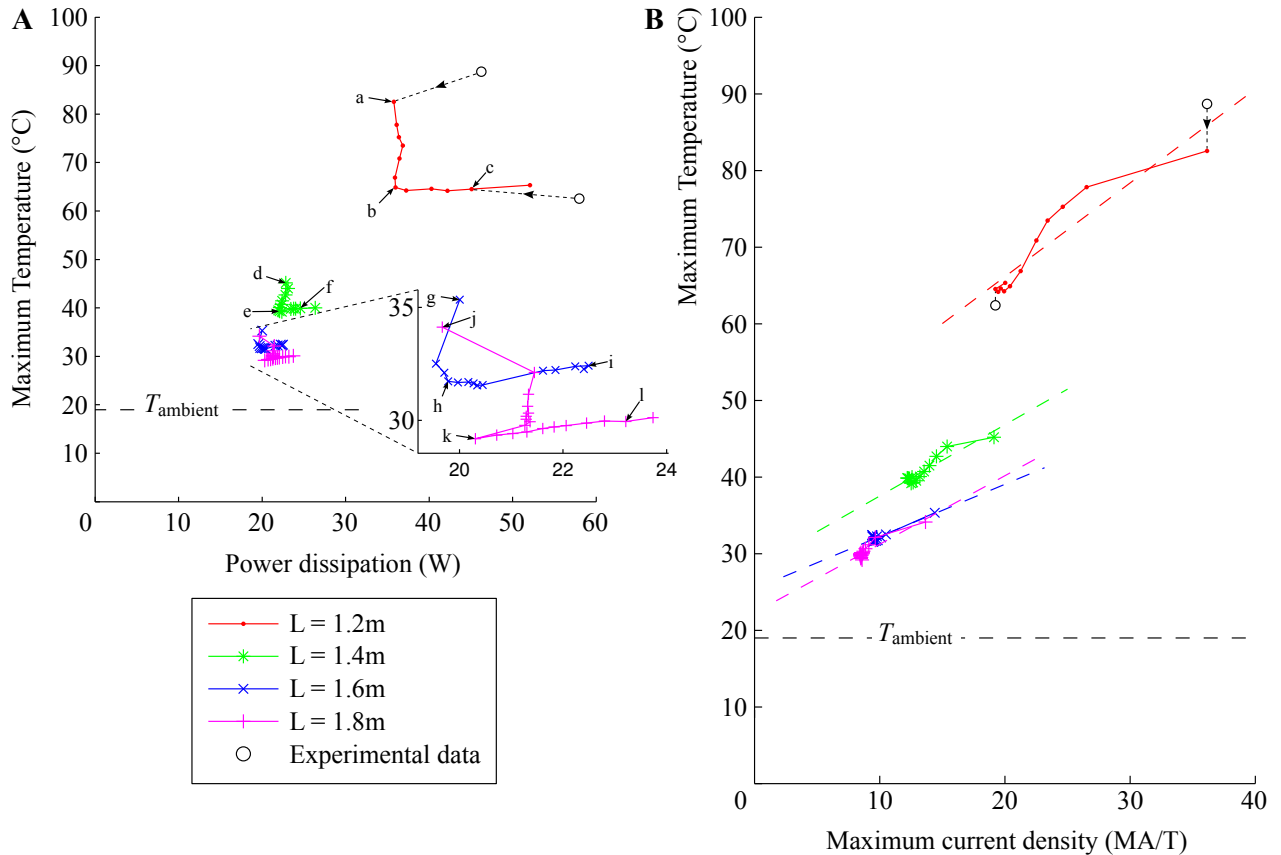


Figure 8: Measured and simulated maximum temperature versus total power dissipation in the coils, A. All coils shown in Fig. 3 are labelled and inset shows data for the two longest coils in detail. Maximum temperature is plotted against maximum current density in B. Linear fits are added to the data in B.